
Article:
Alborzi, E. orcid.org/0000-0002-2585-0824, Parks, C.M., Gadsby, P. et al. (3 more authors) (2020) Effect of reactive sulfur removal by activated carbon on aviation fuel thermal stability. Energy & Fuels, 34 (6). pp. 6780-6790. ISSN 0887-0624

https://doi.org/10.1021/acs.energyfuels.9b04370

Fossil Fuels

Effect of Reactive Sulfur Removal by Activated Carbon on Aviation Fuel Thermal Stability

Ehsan Alborzi, Christopher M. Parks, Phil Gadsby, Abdolkarim Sheikhansari, Simon G. Blakey, and Mohammed Pourkashanian

Energy Fuels, **Just Accepted Manuscript** • DOI: 10.1021/acs.energyfuels.9b04370 • Publication Date (Web): 21 May 2020

Effect of Reactive Sulfur Removal by Activated Carbon on Aviation Fuel Thermal Stability

Ehsan Alborzi,*,† Christopher M. Parks,† Phil Gadsby,† Abdolkarim Sheikhansari,† Simon G. Blakey,‡ and Mohammed Pourkashanian†

†*Department of Mechanical Engineering, The University of Sheffield, Sheffield S3 7HF, UK*

‡*Department of Mechanical Engineering, The University of Birmingham, Birmingham B15 2TT, UK*

E-mail: e.alborzi@sheffield.ac.uk

Abstract

The effect of reactive sulfur removal from a Jet A-1 fuel with marginal thermal stability on surface deposition propensity is reported. The sulfur removal was achieved through adsorptive treatment of the fuel with activated carbon. The treated fuel was assessed for surface deposition propensity using a High Reynolds Thermal Stability (HiReTS) test device. It was found that activated carbon has a strong adsorption capacity for removal of reactive sulfur and Fe components from the fuel. This resulted in a substantial reduction of surface deposition propensity of the Jet A-1 fuel.

Density Functional Theory(DFT) was used to investigate the role of reactive sulfur and Fe on thermal oxidative stability. Mechanistic pathways for intervention of these class of species with hydroperoxides are proposed.

Introduction

Chemistry of fuel autoxidation

Gas turbine fuels undergo thermal stress in fuel lines prior to the combustion chamber. The temperature of the bulk fuel increases as it passes through the engine fuel supply system. This initiates a multitude of chemical reactions in the bulk fuel.[1] These chemical reactions collectively result in the formation of a number of soluble and insoluble complex organic molecules(e.g., molecules composed of hydrocarbons, sulfur, nitrogen and oxygen).[2] These species ultimately participate to the formation of solid carbon deposits, on the surface of the fuel system. The solid carbon deposits can obstruct filter screens or fuel nozzles, cause disruption to the flow of fuel, and result in breakdown in the operation of specific engine components.

It is known that aviation fuel contains approximately 70 ppm of dissolved molecular O_2(at equilibrium with air, under atmospheric pressure and at room temperature). In general, the presence of molecular O_2 and heat results in a chain reaction in the liquid hydrocarbons, known as autoxidation.

The autoxidation of liquid hydrocarbons has been extensively studied for model fuels, e.g., single component hydrocarbons with the carbon atom numbers in the range of petroleum based jet fuel (C_{10}-C_{12}). The results of these studies demonstrate that the autoxidation reactions proceed through a free radical mechanism.[3–6]

Hydroperoxides are primary autoxidation products but also are found at micro-molar concentrations in Jet-A1 during the storage period.[7] There is no general consensus in the literature to define a maximum admissible concentration for hydroperoxides in jet fuels; we found only one report[8] which refers to an informal maximum level of hydropeoxides in jet fuel as 8

ppm(the military specification peroxide limit). However, it is known that the formation of hydroperoxides during fuel storage period is an inevitable slow process. These species partly undergo thermal decomposition and are mainly catalysed by the intervention of complexes of dissolved metals such as Cu, Fe and Mn.[7,9] However, the underlying chemical interactions of hydroperoxides with dissolved metals is not clearly understood.

Moreover, the presence of sulfur species in jet fuels can both slow the oxidation process and increase the amount of deposits formed. The first observation suggests that sulfur compounds can inhibit the formation of radicals, which are known to accelerate the autoxidation process. The second suggests that a further mechanism can occur which leads to the formation of species which accelerate the formation of deposit precursors. However, the exact nature of how sulfur species increase the amount of deposits is unknown. On the basis of experimental observations, it is believed that reactive sulfur can react with hydroperoxides in a non-radical mechanism to produce alcohols and oxidised sulfur compounds.[10] It is also reported that reactive sulfurs and products of phenolic species in association with indoles and/or carbazoles contribute to the surface deposition.[3,7]

We previously reported that self-reaction of hydroperoxides is a thermodynamically viable chemical pathway in thermally stressed liquid hydrocarbons, in the range of petroleum-based jet fuels. .[11] Our quantum chemistry calculations suggested that the probability of this class of reaction, during the autoxidation, is higher than thermal decomposition reaction. The self-reaction of hydroperoxides is also suggested by Bateman et.al[12] for liquid phase autoxidation of hydrocarbons. In general, reactions involving hydroperoxides results in the formation of a large number of oxygenated products including alcohols, aldehydes, ketones, carboxylic acids, per-acids and etc.[6]

In addition, we showed that treatment of a Jet A-1 fuel(with marginal thermal stability) by

zeolites 3.7Å and 4.5Å resulted in a substantial improvement in surface deposition propensity. Study with a model fuel doped with several polar species showed a strong adsorption a number of heteroatomic species by zeolite . The heteroatomic species included linear C6- alcohol, aldehyde, ketones, aniline, Butylated hydroxytoluene (BHT), Fe-naphthenate($Fe(Nap)_2$) and dibuthyl disulfide(DBDS).[11]

This article aims to:

- demonstrate the impact of adsorption of reactive sulfur(by activated carbon) on reduction of surface deposition propensity of a Jet A-1 fuel with marginal thermal oxidative stability. It is worth mentioning that this work is a laboratory-scale; scaling-up for larger applications and higher level of technology readiness requires serious engineering considerations and was not part of this study.

- propose an explicit chemical pathway for the role of sulfur in reaction with hydroperoxides in the course of liquid autoxidation using model chemical species.

- propose an explicit chemical pathway for the role of dissolved-Fe in reaction with hydroperoxides in the course of liquid autoxidation using model chemical species.

The backbone structure of activated carbon can be considered as a mixture of graphite-like crystallites and non-organised phase composed of complex aromatic-aliphatic shapes. In general, the structure of an activated carbon can be considered as a stack of aromatic sheets(known as crystallites) which are randomly cross-linked and distributed. These are separated by disorganised carbonaceous matter as well as inorganic matter(ash), originated from the raw material. The crystallites are composed of three parallel plane layers of graphite with a diameter of approximately 2×10^{-9}m.

In the course of preparation of activated carbon, during the activation phase, the spaces between the crystallites will contain less organised carbonaceous matter. The resulting channels through the graphitic regions and the interstices between the crystallites of the activated carbon, along with fissures inside and parallel to the graphitic planes, constitute the porous structure. This presents a large surface area; with three categories of pore size including micropores(with a pore width of less than 2×10^{-9}m), mesopores(with a pore width of $2-50\times10^{-9}$m) and macropores(with a pore width of bigger than 50×10^{-9}m).

A high surface area and an adequate pore size distribution are necessary conditions for a carbon adsorbent to perform well in a particular application. Furthermore, the carbon atoms at the edges of the basal planes are unsaturated carbon atoms with unpaired electrons. These sites can potentially bond with non-carbonaceous species such as oxygen-containing surface groups. In addition to the oxygen-containing groups, nitrogen-containing groups can be found on the edge of activated carbon. However, not all of these groups are present on a activated carbon simultaneously. Although, the surface sites with functional groups occupies only a small proportion of the total surface area of activated carbon, a wide range of chemical species can be adsorbed by this type of sorbent. These include aniline,[13] phenol,[14] ethyl alcohol[15] carbonyl species,[16] carboxylic acids,[17]Fe ions[18] and diethyl sulfide.[19]

Fundamental understating of the mechanisms of interactions jet fuel constituents and activated carbon is beyond the scope of this article.

Experimental Work

Baseline fuels and chemical composition

In a similar way as in our previous work,[11] three types of baseline fuels were used in the work presented here for the comparative analysis. These include two types of Jet A-1(one with a marginal thermal stability(sample A) and the other one with high thermal stability(sample B) and a surrogate fuel (a polar-free solvent composed of 5 normal paraffins in the range of C_{10} to C_{14}). The composition of major hydrocarbon building blocks and the most important deposition related species of the baseline fuels are shown in table1.

For the hydrocarbon speciation, reactive sulfurs(sulfides and disulfides) and antioxidants, the Jet A-1 fuel samples were analysed using a test method developed by Intertek UK. In this method sulfur-containing molecules and group types were identified using an Agilent 7890 N gas chromatograph(GC) with a Zoex thermal modulation and an Agilent 355 sulfur chemiluminescence detector.

Quantitative analysis of sulfur classes was performed via normalisation to the total content of sulfur(determined by combustion), followed by UV-Fluorescence. A two dimensional gas chromatography separated sulfur-containing classes, on the basis of the boiling points and polarity. Consequently, it was possible to elute the benzothiophenes and dibenzothiophenes in two well-defined bands, separated from the band of thiophenes, sulfides and mercaptans.

Hydrocarbon speciation was carried out using UOP Method 990-11. The polar nitrogen was measured externally by University of Dayton Research Institute (UDRI), using multidimensional gas chromatography time of flight mass spectrometry, following the analytical method reported in the reference.[20]

Dissolved metal analysis was performed in our lab using a calibrated Spectro-Ciros-Vision ICP-OES instrument. The total concentration of hydroperoxide in the baseline fuels were quantified in our lab, following the test method reported in the reference.[21]

Table 1: Composition of major hydrocarbon constituents along with sulfur, polar nitrogen, hydroperoxides and dissolved metals for the baseline fuels

		Baseline Fuel	
	Fuel sample A	Fuel sample B	Polar-free solvent
Chemical composition		**Concentration**	
n-Paraffins	20.67% m/m	19.56% m/m	97.2% m/m
iso-Paraffins	24.77% m/m	25.83% m/m	NA
cyclics	30.84% m/m	31.92% m/m	NA
Alkylbenzenes	16.18% m/m	15.12% m/m	1.1 %
Indans and tetralins	2.15% m/m	2.1% m/m	NA
Naphtalenes	1.33% m/m	1.28% m/m	NA
Antioxidant	25 mg/l	25 mg/l	NA
Acidity	0.08 $mgKOH/100g$	0.072 $mgKOH/100g$	NA
Thiols, Sulfides and Disulfides	835 mg/kg	812 mg/Kg	NA
Polar Nitrogen	12 mg/kg	12 mg/kg	NA
Total hydroperoxides	18.6 μM	4.1 μM	2.5 μM
Dissolved Fe	115 *ppb*	110 *ppb*	NA
Dissolved Cu	50 *ppb*	38 *ppb*	NA
Dissolved Zn	48 *ppb*	64 *ppb*	NA

Assessment of fuel thermal oxidative stability

High Reynolds Thermal Stability(HiReTS) device based on ASTM D6811-02 test method was used to asses the thermal stability of the baseline fuels as well as the treated fuels, for comparative analysis. In this, an aerated test fuel was filtered and pumped through an electrically heated capillary at turbulent flow regime. The capillary tube was controlled to maintain a constant fuel temperature of 290 °C at the capillary tube exit.

The external surface of capillary was blackened to create a high thermal emissivity in such away that a pyrometer be able to measure the real-time changes along the capillary wall temperature. During the HiReTS test, temperature increased in a non-linear trend along the external surface of the capillary tube. This was due to the formation of the insulative layer of carbonaceous deposits at the inner surface of capillary tube.

The temperature in the localised areas was captured at discrete measurement points, along a small section of the capillary. This was to create a time-profile of temperature rise along the tube wall. We defined an arbitrary number as the HiReTS number, as shown in equation1. This number corresponds to the thickness of deposit inferred from the changes to the thermal conduction between fuel and wetted wall. The calculation of HiReTS number employs the difference between the final and minimum ΔT measurement in the data set generated at each of the measurement positions. The total HiReTS number was calculated by summing this difference at each measurement position as shown in equation1. The test condition used in the HiReTS device is presented in table2.

$$\sum_{n=1}^{n=12} (\Delta T_{Final} - \Delta T_{min}) \tag{1}$$

Table 2: Test conditions in HiReTS

Test Parameters	**Values**
Flow Rate(ml/min)	35
Bulk fuel temperature at tube outlet(°C)	290
Test Pressure(MPa)	2.0
Test Time(min)	120
Number of positions measured per scan(n)	12
Scans per test	25
Distance between measured position(mm)	2.5
Fuel aeration time(min)	12
Scan time(min)	5

Adsorptive fuel treatment

A packed bed reactor was used to explore the effect of activated carbon on polar species removal. The packed bed reactor consisted of a 1 m stainless steel tube with a 2.54 cm inner diameter and 6 K-type thermocouples inserted equally distant along the tube for data logging. The distance between two adjacent thermocouples was 15 cm. Subsequently, the impact of fuel treatment by activated carbon on fuel thermal stability was assessed in HiReTS device. .

The tube was centrally placed inside a temperature controlled furnace. A proportional integral derivative (PID) controller was used to heat the furnace up to a fixed set point temperature prior to each experiment. Once system reached thermal equilibrium, the tube reactor was filled up with the adsorbents and fuel and then located inside the furnace. It is important to note that if the tube was connected to the pump prior to the furnace warming up, the time needed to fill the tube with fuel would have been significantly longer. Therefore, adsorption capacity of the solid adsorbents could have been disturbed through longer interactions with the fuel. In the absence of cooling effect, once the furnace reached the thermal equilibrium, the time needed for fuel inside the tube to reach to the set point temperature was faster compared to the flowing system. This helped to reduce the effect of gradual temperature rise on the air solubility in fuel.[22]

The amount of adsorbent was fixed in such away to fill up the isothermal region of the packed bed reactor. Subsequently, a fixed flow rate of 5 ml/min was set through a pump as a part of solvent delivery system in a high performance liquid chromatography(HPLC). This was to provide a long residence time for the adsorption process in the bed.

The level of dissolved O_2 was monitored in-line by an optical oxygen sensor(Inpro 6860, Mettler Toledo) during each test. The position of the oxygen sensor was approximately 1 m downstream of the tube reactor. Since a standard complete HiReTS test requires 5 L of jet fuel(including test volume and rinsing), each test in the packed bed reactor took approximately 17 h to obtain sufficient volume for thermal stability assessment in the HiReTS.

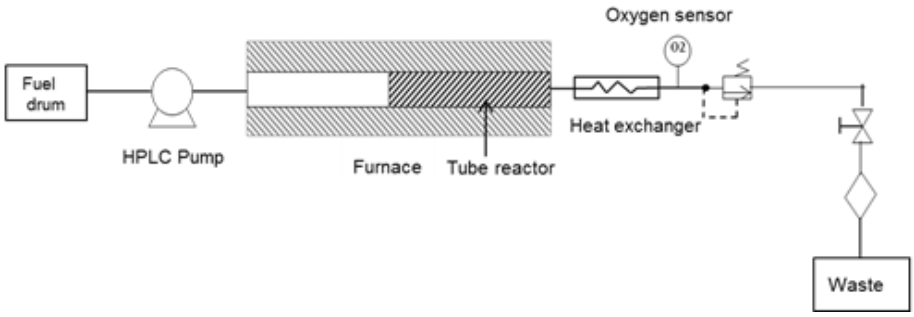

Figure 1: Schematic of packed bed reactor

To explore one by one interaction of the polar species with activated carbon and comparison with the adsorption by zeolites, the surrogate fuel was doped with the known amount of polar species individually. This was followed by the adsorptive treatment using 10 ml cartridges, filled with 1 g the sorbent. The cartridges were connected to a vacuum manifold so that a fixed flow rate of 1 drop/s was set for the treatment. The list of polar species and their concentrations in the surrogate fuel is shown in table3.

The higher concentrations of polar species were added to the surrogate fuel to minimise the quantification errors. It is worth to note that, although the selected polar species in this work shared the same functional groups in their molecular structures with the polar species in a typical Jet A-1, their molecular weights were significantly lower. The choice of polar species in surrogate fuel in this work mainly was based on the availability of these chemical species in the market. Finding more representative chemical species as of those identified in jet fuel is challenging. The use of less representative chemical species in the study of fuel behaviour is frequently reported in the literature based on the scope of the works. Concentration of polar species in the treated samples were measured by gas chromatography with the exception of $Fe(Nap)_2$ which was quantified by ICP-OES.

Table 3: List of polar species and concentration in model fuel

Polar species	Supplier	Concentration / ppm
Hexanoic acid(analytical grade)	Sigma-Aldrich	200
Hexanol(analytical grade)	Sigma-Aldrich	200
Hexanal(analytical grade)	Sigma-Aldrich	200
Hexanone(analytical grade)	Sigma-Aldrich	200
Cumene hydroperoxides(analytical grade)	Sigma-Aldrich	200
Dibutyl disulfide(DBDS)(analytical grade)	Sigma-Aldrich	200
Phenylamine(aniline)(analytical grade)	Sigma-Aldrich	200
Butylated hydroxytoluene(BHT)(analytical grade)	Sigma-Aldrich	200
0.012-0.015 mM Fe-naphthenate($Fe(Nap)_2$(12% wt)	Fisher Scientific	0.2

Quantum chemistry

All calculations were performed using Gaussian 09 software, version D.01 with Gaussian-supplied versions of BLAS[23] and ATLAS. All calculations employed the use of the B3LYP functional.[24–30]The cc-pVDZ[24] basis set was used for all non-metallic elements with SDD being employed on iron.[31]

In all calculations the solvent was accounted for using the PCM method as implemented in Gaussian.[32] The solvent parameters for dodecane were used for all calculations. Geometry optimizations were confirmed as local minima by the absence of imaginary frequencies in the vibrational spectra. All transition states were confirmed via the presence of one imaginary frequency corresponding to the saddle point, as expected. Intrinsic reaction coordinate (IRC) scans were conducted on all transition states to confirm they connected the correct reactant and product. Transition states were optimized using the QST3 method as implemented in Gaussian 09.[33]

An ultrafine grid was employed for all calculations with no symmetry constraints. All structures were calculated as singlets with the HOMO and LUMO orbitals mixed (guess=mix option) in order to break the symmetry of the system. Free energies were calculated using the Grimme quasi-harmonic entropy correction[34] using the GoodVibes script.[35]

From the equations below, the Arrhenius equation can be linked to the enthalpy and entropy of the reactions. The activation energy(Ea) was taken as the enthalpy change between the reactants and the transition states, and pre-exponential factor(A) was obtained from the entropic term.

The rate of a chemical reaction can be given by the Arrhenius equation, as shown in equation2.

$$k = A\ exp(\frac{-Ea}{RT}) \tag{2}$$

The rate constant can also be written as illustrated in equation 3, where the pre-exponential factor has been split up into a temperature dependent component and an entropic component.

$$k = \frac{KbT}{h} exp(\frac{\Delta S}{R})\ exp(\frac{-Ea}{RT}) \tag{3}$$

In a solvent, the activation energy can be substituted for the enthalpy of activation as presented in equation4.

$$k = \frac{KbT}{h} exp(\frac{\Delta S}{R})\ exp(\frac{-\Delta H}{RT}) \tag{4}$$

This indicates that the Arrhenius pre-exponential factor can be calculated using equation5.

$$A = \frac{KbT}{h} exp(\frac{\Delta S}{R}) \tag{5}$$

Results and Discussion

Treatment with activated carbon- impact on thermal stability

The surface deposition propensity of the baseline fuels, assessed in the HiReTS tube, is shown in figure 2. It can be seen that the polar-free solvent has the highest thermal oxidative stability when compared to the other two fuel samples. Such a high thermal stability is attributed to the absence of polar species(e.g., naturally occurring antioxidants, polar nitrogens, reactive sulfurs and dissolved metals).

As discussed in our previous work,[11] figure 2 illustrates that the treatment of fuel sample A with zeolites resulted in a substantial thermal oxidative stability improvement. We suggested that this was attributed to the partial adsorption of some of the polar species by zeolites. This was supported by the partial adsorption of some of the heteroatomic species from spiked model fuel by zeolites, as presented in figure 3. Furthermore, we discussed that zeolites exhibited a strong adsorption of Fe-bonded molecules from Jet A-1 .

Treatment of fuel sample A by the activate carbon resulted in a greater decrease in deposition propensity than zeolite 3.7 Å, as shown in figure 2. In addition, it can be seen that deposition propensity of the same fuel sample treated with zeolite is manifested by a much shorter induction period when compared with the case treated with the activated carbon.

The results shown in figure 3 illustrate that as opposed to the zeolites, activated carbon exhibited a strong adsorption of DBDS.

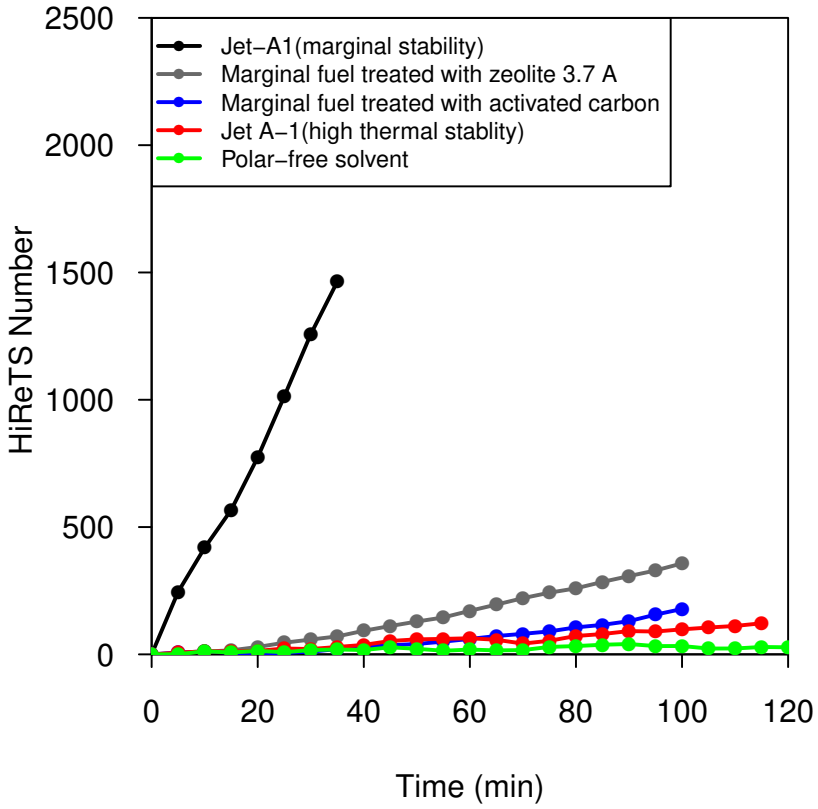

Figure 2: Comparison between the effect of polar species removal by zeolites and activated carbon on deposition propensity of marginal fuel

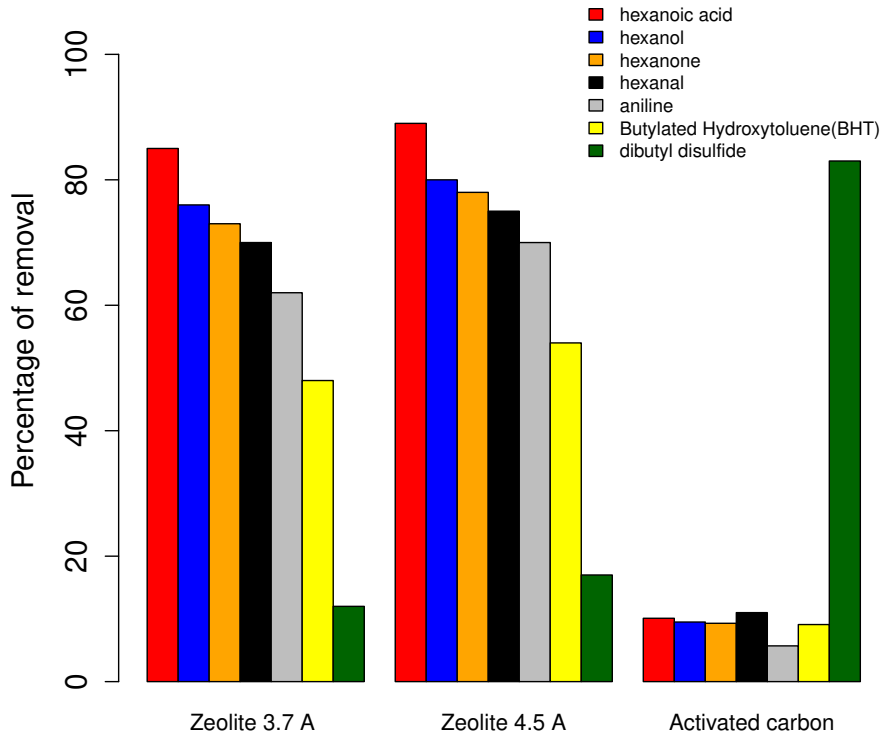

Figure 3: Adsorption of polar species by zeolites 3.7Å, 4.5Å and activated carbon

.

The observed differences in deposition behaviour for fuel sample A prior to, and after treatment with zeolites and activated carbon encouraged us to carry out a concurrent computational investigation. The aim of this was to gain insight into how Fe-bonded species and reactive sulfur might affect both autoxidation and deposition rates. This will be discussed later in this section.

Interpretation of polar species removal from model fuel in the packed bed reactor

The overall rate of adsorption in a multicomponent mixture is controlled by several distinct resistances to mass transfer. In fact, without detailed analysis coupled with appropriately designed experiments, it is not clear which resistance is rate controlling. Therefore, although direct measurement of the transient uptake curve of individual species by a bed can provide a simple method of studying adsorption kinetics, the interpretation of such data presents more difficulties than might be expected.

This is not in scope of this article to perform a mathematical modelling for comprehensive analysis of multicomponent adsorption of the polar species in the packed bed reactor. Alternatively, in a simplified way, we focused our attention on comparison between dynamic behaviour of the bed of activated carbon and combined bed in overall adsorption of each polar species over time. This is explained from the results shown in figure4-a and figure4-b. In these figures % concentration of polar species in the spiked model fuel as function of time is presented as an indication for the species adsorption.

- **Packed bed of activated carbon**

The results in figure4-a indicate that adsorption of DBDS and $Fe(Nap)_2$ by activated carbon from the spiked model fuel had started faster when compared with other polar species. It can be seen that approximately after 60 min of the experiment, the adsorption of of DBDS and $Fe(Nap)_2$ started with the same rate. However, adsorption of DBDS became faster after 100 min of the experiment.

Despite faster adsorption for DBDS, both species exhibited the same maximum level

of uptake and an invariant uptake period was observed for the rest of experiment; the adsorption of other species by the bed of activated carbon was insignificant. Excluding $Fe(Nap)_2$, this was in agreement with the results of species adsorption in cartridges(figure3).

Despite strong adsorption of oxygenated species, aniline and phenolic components by activated carbon, as reported in the literature section of this article, in our study adsorption of DBDS and $Fe(Nap)_2$ dominated. Further research is required to elucidate the competitive adsorption between various chemical species with activated carbon. However, this is beyond the scope of this article.

- **Combined packed bed(activated carbon + zeolite 3.7 Å)**

The results in figure4-b show that after approximately 60 min of the experiment, the adsorption of DBDS, Fe(Nap)2 and oxygenated species began. However, the rate of adsorption of these species is different from one another with the DBDS having the highest and oxygenated species lowest rate.

It was noted that maximum uptake of DBDS and $Fe(Nap)_2$ achieved by the combined packed bed, was approximately the same as the one corresponding to the activated carbon. This is likely to be attributed to the fact that in the combined packed bed, the activated bed was placed before the zeolite bed. Therefore, it appears that the adsorption of DBDS and Fe(Nap)2 occurred with no interference due to physisorption or chemisorption by zeolite.

It is interesting to note that the maximum uptake of oxygenated species was approximately the same as in the case of adsorption in packed bed of zeolite, as shown in our

previous work.[11] However the rate of adsorption of this class of species was slower in the combined packed bed.

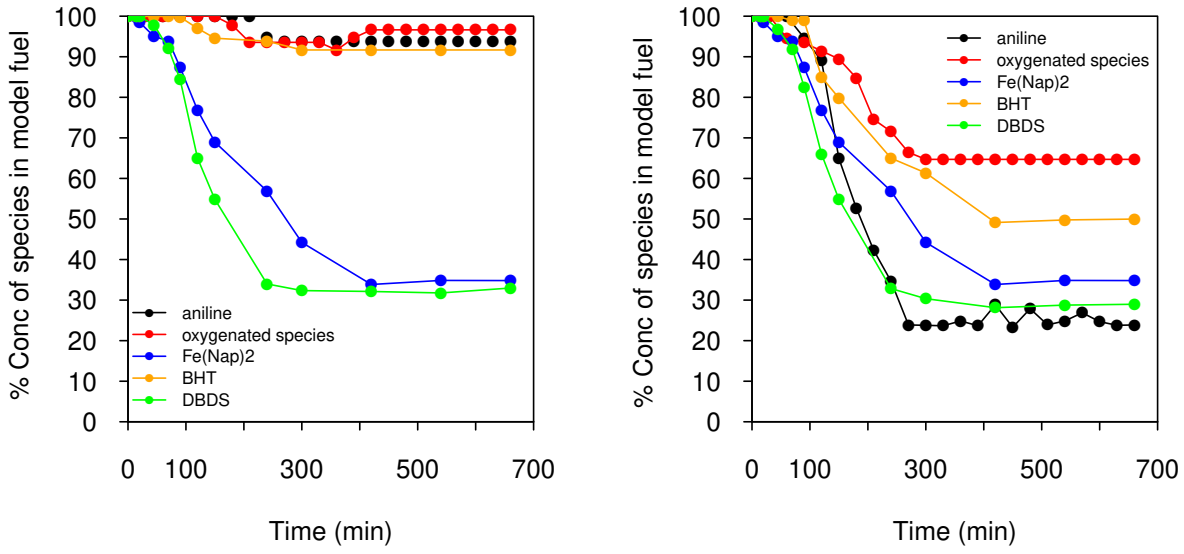

(a) activated carbon (b) combined bed

Figure 4: Adsorption of Fe(Nap)2, DBDS, BHT, aniline and oxygenated products from spiked model fuel in the packed bed reactor, filled with activation carbon(a) and a combined bed composed of activated carbon and zeolite 3.7 Å

Role of dissolved Fe in fuel thermal oxidative stability

Subsequently, we decided to employ quantum chemistry to preliminary investigate potential mechanistic pathways where Fe complexes could affect thermal stability of fuel.

We first probed the potential structures that the $Fe(Nap)_2$ complex could adopt in solution. Figure 5 shows the initial geometries selected for optimisation.

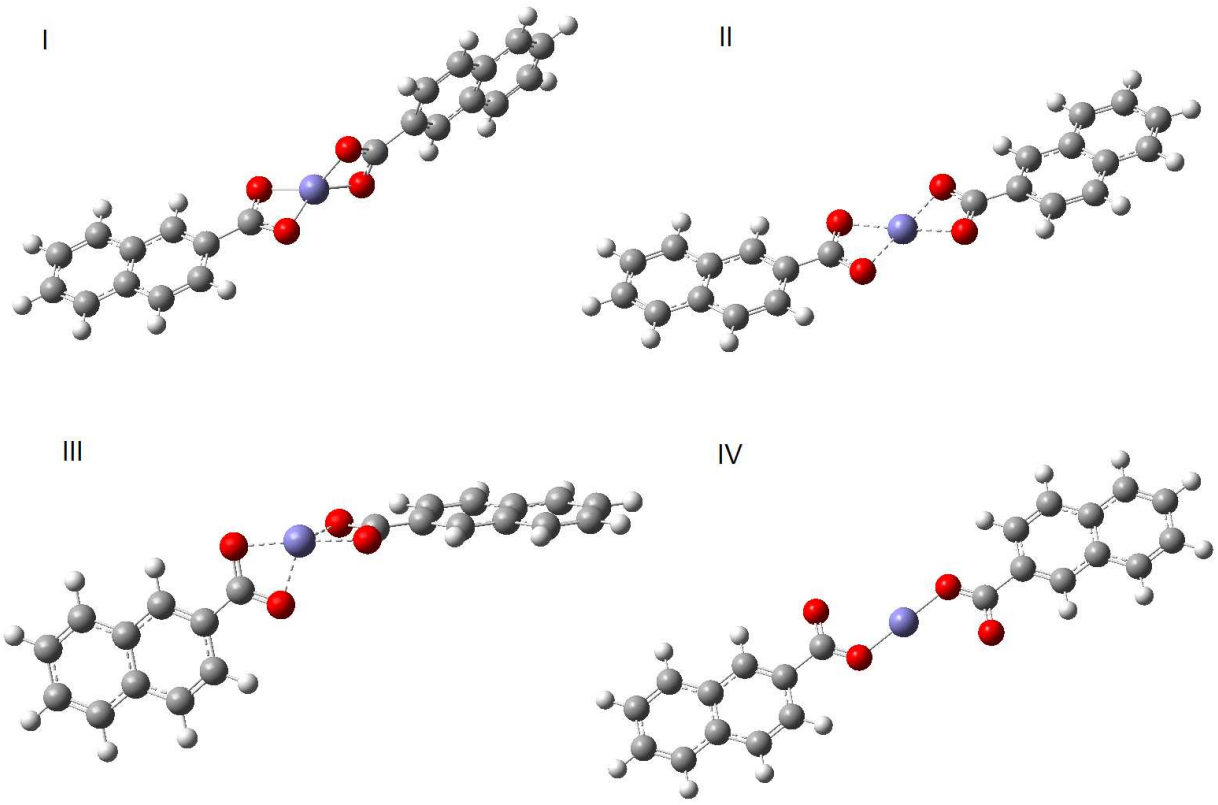

Figure 5: Four initial geometries investigated for $Fe(Nap)_2$. (I) Approximately tetrahedral geometry. (II) Planar geometry. (III) Distorted octahedral geometry (IV) Linear geometry with the ligands binding to the metal in a monodentate fashion.

Following optimisation, the structure with tetrahedral geometry (I in figure 5) collapsed to the structure II. The structure with the naphthenate ligands acting as monodentate ligands (structure IV) also collapsed to the structure II.

The most stable geometry was found to be structure III, which was 11.7 kcal mol^{-1} more stable than the next most stable structure. Here, the geometry around the Fe centre is approximately octahedral with two unoccupied sites(cis to one another). The Fe-O bond lengths are 1.95 Å for the bond trans to an occupied site and 2.00 Å for the remaining Fe-O bonds(trans to one another).

Our next consideration was to explore how this low energy reactant structure could facilitate

the fission of hydroperoxides in the fuel. It is generally accepted that homolytic fission of hydroperoxides requires 40-45 kcal mol^{-1} and proceeds through a barrierless process. Therefore, the Fe complex cannot act as a catalyst in the fission of hydroperoxides(as there is no barrier present which can be lowered). Hence, the presence of the Fe complex must provide an alternative pathway to produce radicals.

The hydroperoxide selected for investigation here was cumene hydroperoxide (CHP), as a representative species for aromatic hydroperoxides that could potentially be found in Jet A-1.

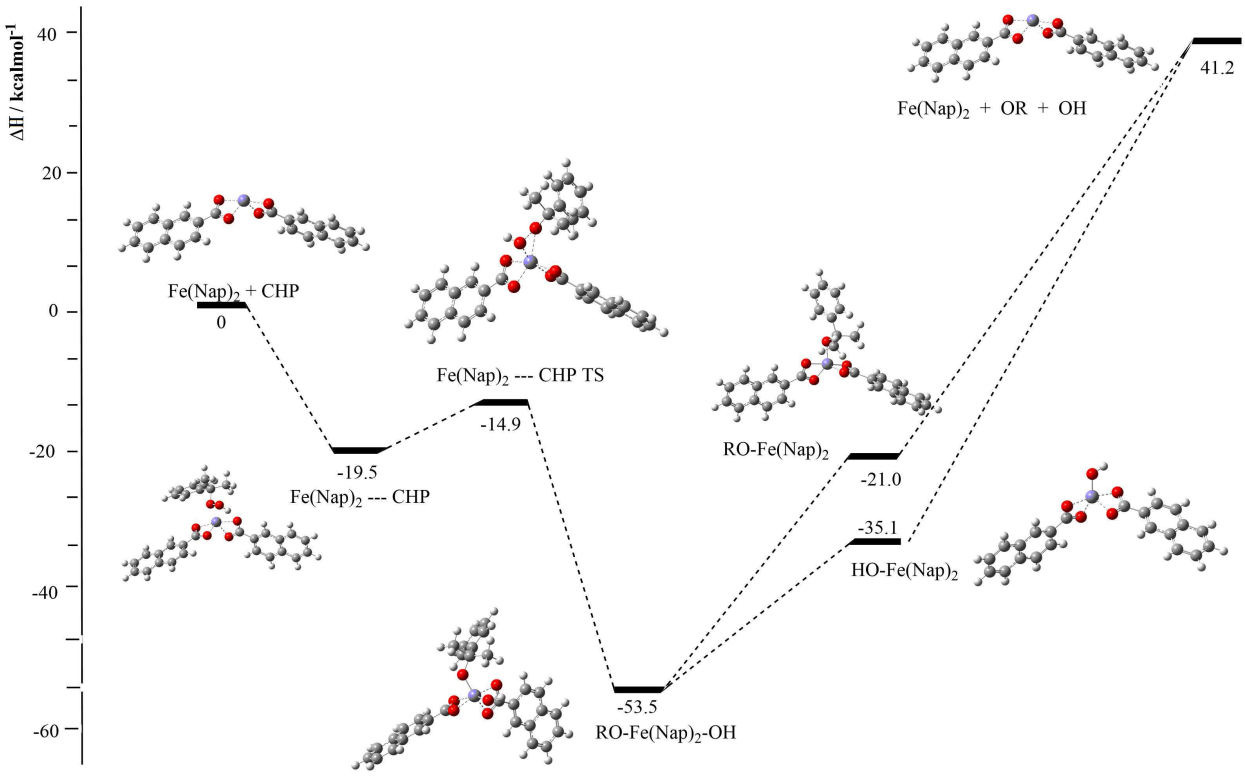

Figure 6: Energy profile for the reaction of $Fe(Nap)_2$ and CHP

Figure 6 shows a DFT-calculated energy profile for the reaction of $Fe(Nap)_2$ with CHP. The pre-reaction complex(labelled as $Fe(Nap)_2$—CHP) is defined as the structure immediately preceding the transition state whereby the reactants are in close proximity. In this structure the hydroperoxide binds with the Fe complex through the alkoxy oxygen in R**O**OH with an

Fe-O distance of 2.06 Å(left structure in figure 7).

The hydroxy hydrogen on the hydroperoxide shows a hydrogen bond to one of the naphthenate ligands with a distance of 1.95 Å. In the transition state(labelled as $Fe(Nap)_2$—CHP TS), the O-O bond has lengthened from 1.46 Åto 1.87 Å(right structure in figure 7).

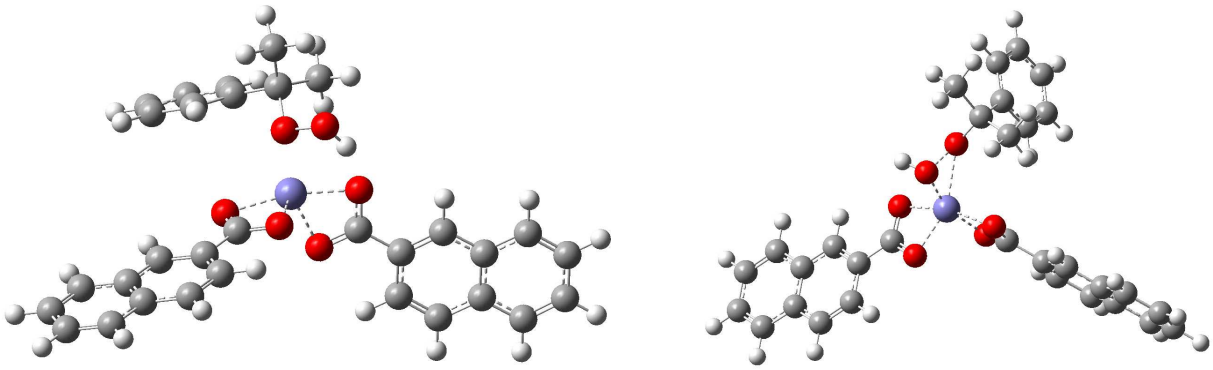

Figure 7: Left: pre-reaction complex. Right: Transition state geometry

Figure 6 indicates that the activation energy for the reaction is 4.6 kcal mol^{-1}. Also, the results show that in the product complex, the hydroperoxide has been cleaved and the constituent radicals are now bound to the metal centre in a cis arrangement. The product complex is 53.5 kcal mol^{-1} more stable than the separated reactants.

Next, we investigated how this product complex might release radicals. This was achieved through the optimisation of three further species including HO-$Fe(Nap)_2$ + RO$\cdot$, RO-$Fe(Nap)_2$ + .OH and $Fe(Nap)_2$ + OR$\cdot$ + .OH. The first two species are formed through the loss of either OR$\cdot$ or OH$\cdot$ respectively from RO-$Fe(Nap)_2$-OH. The final species is the regenerated metal complex that has lost both radical species.

An interesting observation from the results of figure 6 is that the release of the RO$\cdot$ over the .OH is preferred by 14.1 kcal mol^{-1}; release of both radicals from the product complex sequentially is endoergic by 92.9 kcal mol^{-1}. This suggests that whilst in the presence of Fe

complex, hydroperoxides can be successfully cleaved, release of radicals from the product species is less likely. It is worth noting that these findings were based on the model species, so further research is required to explore the behaviour of wider class of hydroperoxides and metal complexes in fuel which is outside the scope of this article.

Reaction of RO-Fe(Nap)$_2$-OH with dodecane

Another potential route to radical formation could be the reaction of low energy product complex with the bulk fuel(species in great excess). In theory, either of the bound radical species (RO$\cdot$ or .OH) could potentially react with the bulk species which would result in the production of an alkyl radical (R$\cdot$) and either an alcohol (ROH) or water (HOH).

The two decomposition routes are schematically shown in figure 8 for the reaction of RO-Fe(Nap)$_2$-OH with dodecane. Dodecane was chosen as a model for bulk species in jet fuel as well as bulk species in the the polar-free solvent.

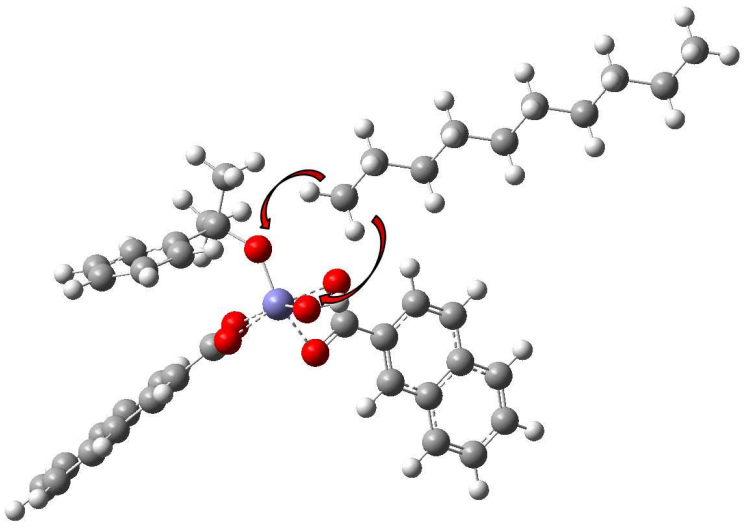

Figure 8: Two potential reactions that could occur between RO-Fe(Nap)$_2$-OH and dodecane.

The energy profile for this reaction is shown in figure 9. Two transition states were initially optimised for each H-transfer reaction to either the hydroxy or alkoxy radical. One involved a reaction at the terminal dodecane carbon atom and the second at the secondary carbon. In each case the reaction at the secondary carbon atom had the lower activation energy. This can be attributed to both the enhanced stability of the generated alkyl radical species and the fact that C-H bonds at secondary carbon atoms are weaker and thus more easy to cleave than those at primary carbon atoms. This is further evidenced by the calculated C-H bond strengths which are 94.4 and 98. 7 kcal mol^{-1} for the terminal C-H and secondary C-H bond respectively.

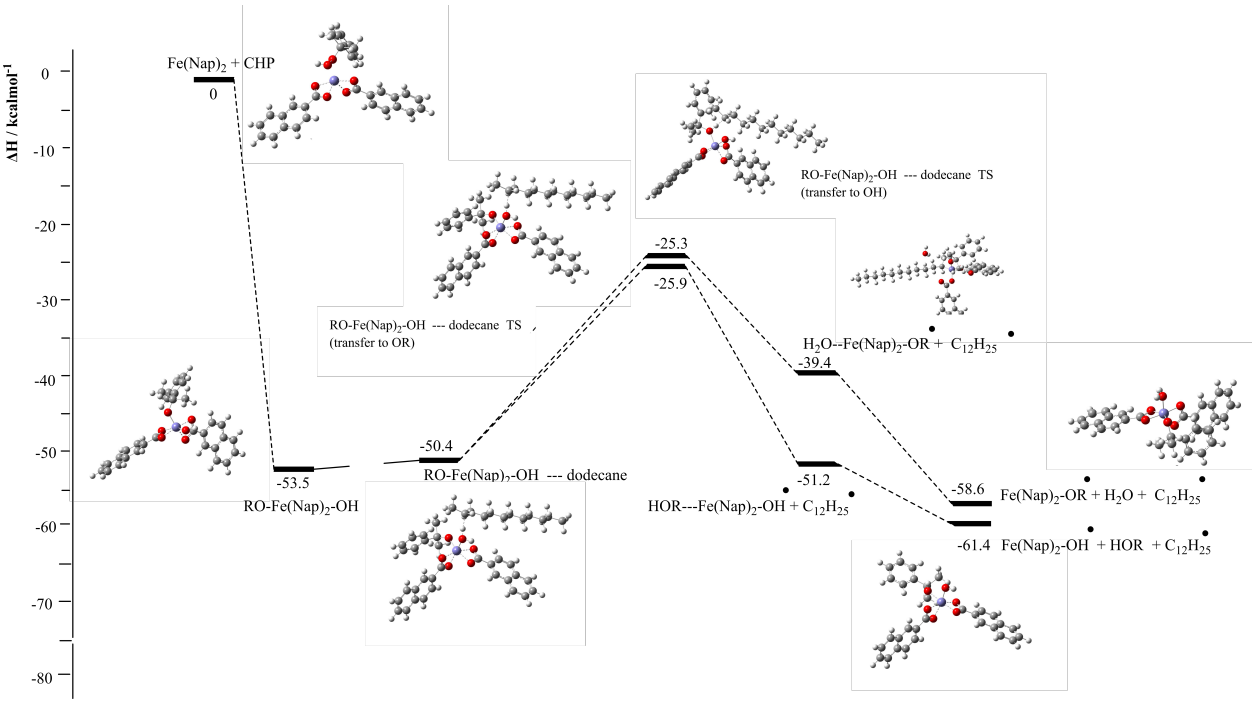

Figure 9: Energy profile for the reaction of RO-Fe(Nap)$_2$-OH and dodecane

As can be seen in table 4, the activation energy for the reaction of RO-Fe(Nap)$_2$-OH and dodecane is lower than that for hydroperoxide fission(thermal decomposition). (25.9 cf. 40-45 kcal mol^{-1}). This result implies that reaction of the low energy Fe product with n-dodecane potentially affords a more favourable route to producing an alkyl radical species in fuels.

Table 4: Activation energies and associated Arrhenius parameters for reaction of RO-Fe(Nap)$_2$OH and n-dodecane to form HOR—Fe(Nap)$_2$OH + $C_{12}H_{25}$

Δ H(kJmol^{-1})	$\Delta S(kJmol^{-1}K^{-1})$	$A(mol, L, s)$
25.9	-21.55	$1.212E8$

Role of reactive sulfur in fuel thermal oxidative stability

As mentioned previously, it is known that reactive sulfur species can react with hydroperoxides through a non-radical mechanism to produce alcohols and oxidised sulfur compounds. Whilst these types of reactions have not been extensively investigated computationally, some studies are present in the literature. Bach et al. demonstrated that hydroperoxides can transfer their hydroxyl oxygen atom via a concerted mechanism to the sulfur species.[36] Zabarnick and coworkers found that the reaction of diethyldisulphide and hydroperoxide was strongly exoergic but had a relatively high activation energy.[37]

It was therefore of interest to investigate how sulfur might interact with hydroperoxides. We used DBDS and CHP as model species for DFT calculations to construct an energy profile of the reaction, as presented in figure 10.

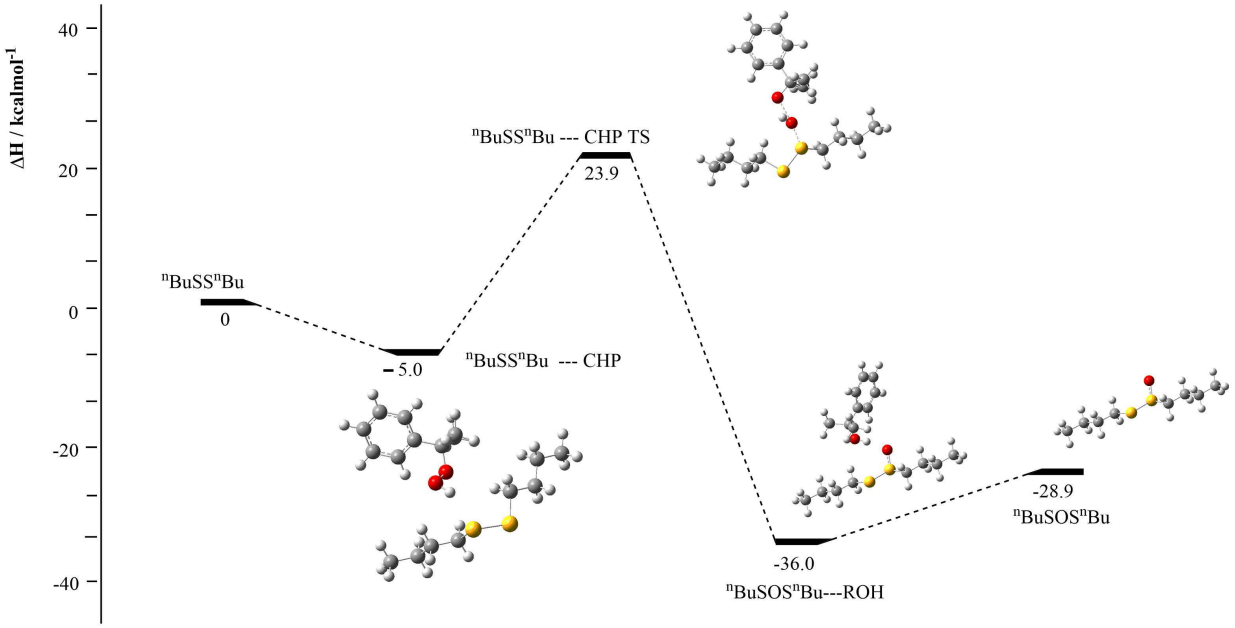

Figure 10: Energy profile for the successive oxidation reactions of CHP to DBDS.

The optimised geometry of the transition state is shown in figure 11. In this structure, the terminal oxygen atom of the hydroperoxide is transferred to the sulfur atom via a concerted mechanism. This proceeds through the rotation of the hydroxyl group in such a way that the hydrogen is transferred back to the reacting hydroperoxide molecule to form an alcohol. The activation energy for this reaction is 28.9 kcal mol^{-1}. Whilst this activation energy is reasonably high, it is still lower than the typical reported values for thermal decomposition of hydroperoxides which is known to occur. The reaction is exoergic with a reaction energy of -36.0 kcal mol^{-1}. Similar activation energies were reported by Zabarnick et. al (26.1 and 28.7 kcal mol^{-1} for reaction of diethyl sulfide and diethyldisulfide with hydroperoxide respectively). The corresponding reaction energies were -26.3 and -27.7 kcal mol^{-1} [37] The small differences in activation energies between their calculated values and the values reported here can be attributed to the different basis set and solvent model employed in the calculations.

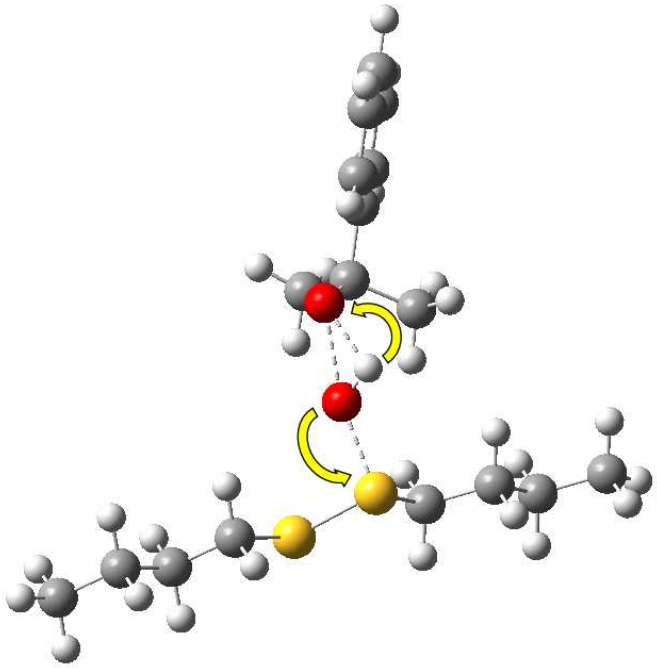

Figure 11: Optimised transition state structure for the reaction of DBDS and CHP.

The oxidised product can potentially undergo successive oxidation reactions with further equivalents of hydroperoxide. As the oxidized product is now unsymmetrical and each sulfur environment is distinct, the oxidation at each sulfur site was first probed. It was found that the second oxidation reaction was more favourable at the previously unreacted sulfur. The energy profile for four successive oxidation reactions is shown in figure 12.

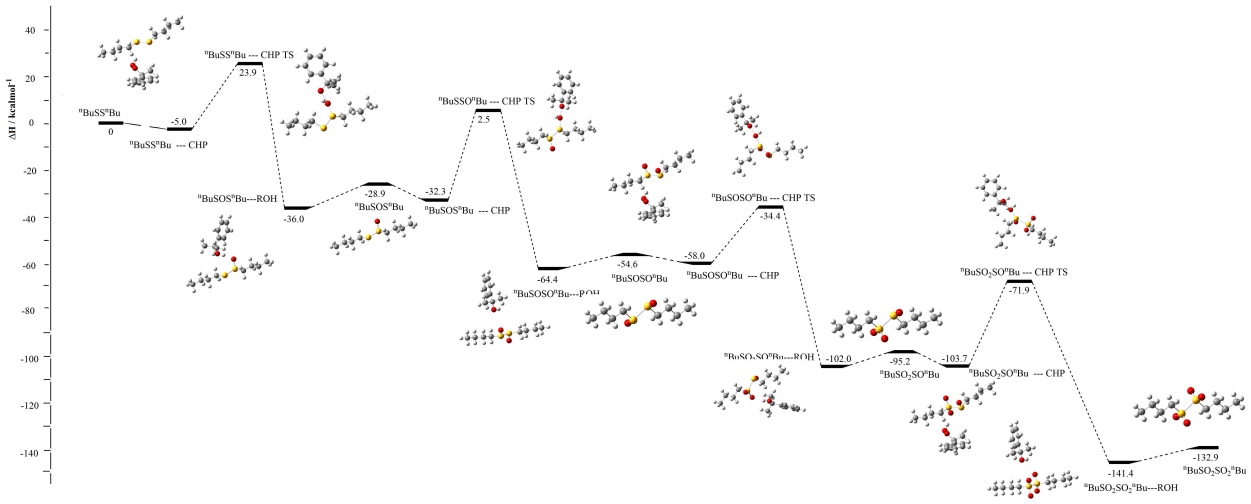

Figure 12: Energy profile for the successive oxidation reactions of CHP to DBDS.

The activation energies for each oxidation reaction are given in table5. They range from 23.6 to 31.8 kcal mol^{-1}. This illustrates that the disulfide species can potentially react with as many as four equivalents of hydroperoxides which in turn produces four equivalents of alcohols. However, one must also carefully consider the proportions of each species present in jet fuel. Each reaction presented here will reduce the remaining peroxide concentration in the fuel. Moreover, the relative proportions of successive oxidised sulfur species will also be appreciably lower than the initial sulfur species present in the fuel. As a consequence of both of these, each successive oxidation reaction will occur at a reduced rate, if they occur at all.

Table 5: DFT-calculated activation energies and associated Arrhenius parameters for four successive oxidations to DBDS

Oxidation reaction	ΔH(kJmol^{-1})	$\Delta S(kJmol^{-1}K^{-1})$	$A(mol, L, s)$
1	28.9	-6.20	2.7E11
2	29.8	-0.66	4.46E12
3	23.6	-5.55	3.80E11
4	31.8	-0.98	3.78E12

As the propensity for further reactions of the oxidised sulfur species is reduced, as a consequence of lower hydroperoxide concentrations, we turned our attention as to whether the

oxidised product of this reaction ($C_4H_9SOSC_4H_9$) could potentially undergo any further relevant reactions. It was noted that the sulfur-sulfur bond length was longer in this species (2.23 Å) when compared to the initial reactant (2.10 Å). This led us to consider whether the sulfur-sulfur bond could undergo thermal homolytic decomposition, in an analogous manner to hydroperoxides.

It was found that the S-S bond dissociation energy is 29.2 kcal mol^{-1}, which is similar to reported literature data for such compounds.[38–40] This is comparable to the energy required to break hydroperoxides into their constituent radicals (normally quoted at 40-45 kcal mol^{-1}). Whilst it is not possible here to provide an exhaustive list of all possible reactions that these radical species might undergo, we have demonstrated a mechanistic pathway through which both hydroperoxides can be consumed and alcohols and acids can be produced. Furthermore, the oxidised sulfur products can even break down homolytically to liberate radicals.

Given that DBDS and $Fe(Nap)_2$ can strongly be adsorbed by activated carbon, it appears that treatment of the fuel sample A by this sorbent reduces the probability of hydroperoxide non-radical decomposition. In such a situation, when the fuel was thermally exposed in the HiReTS tube, thermal autoxidation was controlled by self-reaction and thermal decomposition of hydroperoxides.

Considering that adsorption of DBDS by zeolite is not strong, it is believed that for the case of treatment of fuel sample A with zeolite, thermal degradation of the fuel in the HiReTS tube is predominantly controlled by non-radical decomposition of hydroperoxides.

Conclusions

1. A Jet A-1 fuel sample with marginal thermal stability was treated with activated carbon in a packed bed reactor. It was found that the surface deposition propensity of sample is reduced as assessed by HiReTS.

2. It was found that activated carbon has a strong adsorption capacity DBDS and $Fe(Nap)_2$.

3. Competitive adsorption of various classes of heteroatomic species in a packed bed reactor with activated carbon and a combined bed(composed of activated carbon and zeolite 3.7 Å) was investigated. The heteroatomic species include oxygenated species(e.g.C_6 derived alcohol, aldehyde, ketone, acid), aniline, $Fe(Nap)_2$, BHT and DBDS. It was observed that in the packed bed with activated carbon the adsorption of DBDS and $Fe(Nap)_2$ dominated with a fast kinetic and relatively high uptake capacity. However, adsorption in the combined bed showed a fast kinetic and high uptake capacity for aniline, DBDS and $Fe(Nap)_2$. while BHT and oxygenated species showed a moderate adsorption with a slower kinetic.

4. Mechanistic pathways for the intervention of DBDS and $Fe(Nap)_2$. with hydroperoxide were probed and their impact on fuel thermal oxidative stability was discussed.

5. It was found that DBDS can react with up to four equivalents of hydroperoxides to form a sulfone and alcohols. However, in jet fuel, it is likely that only the first oxidation reaction to be important due to the reducing concentration of peroxides. The oxidised sulfur product can thermally decompose to form two radical species which could potentially participate in deposit formation.

6. $Fe(Nap)_2$ can react with hydroperoxides to form a metal complex containing two radicals, $OH\cdot$ and $RO\cdot$. Dodecane is predicted to favourably react with this complex to form an alkyl radical.

Acknowledgment

This work was supported by the Horizon 2020-Clean Sky 2 programme under research grant agreement 145251. The authors would like to acknowledge Dr.Nicolas Grosejan of Johnson Matthey for solid adsorbent preparation and Mr.Jason Chetwynd-Chatwin of Rolls Royce for technical support.

References

(1) Hazlett, R N, *Thermal Oxidation Stability of Aviation Turbine Fuels*; ASTM, 1991.

(2) Beaver, B.; Gao, L.; Burgess-Clifford, C.; Sobkowiak, M. On the Mechanisms of Formation of Thermal Oxidative Deposits in Jet Fuels. Are Unified Mechanisms Possible for Both Storage and Thermal Oxidative Deposit Formation for Middle Distillate Fuels? *Energy & Fuels* **2005**, *19*, 1574–1579.

(3) Jones, E. G.; Balster, W. J. Phenomenological Study of the Formation of Insolubles in a Jet-A Fuel. *Energy & Fuels* **1993**, *7*, 968–977.

(4) Jones, E. G.; Balster, L. M.; Balster, W. J. Autoxidation of Aviation Fuels in Heated Tubes : Surface Effects. *Energy & Fuels* **1996**, *10*, 831–836.

(5) Kuprowicz, N. J.; Ervin, J. S.; Zabarnick, S. Modeling the liquid-phase oxidation of

hydrocarbons over a range of temperatures and dissolved oxygen concentrations with pseudo-detailed chemical kinetics. *Fuel* **2004**, *83*, 1795–1801.

(6) Denisov, E. T.; Afanas'ev, I. B. *Oxidation and Antioxidants in Organic Chemistry and Biology*; CRC Press, 2005.

(7) Kuprowicz, N. J.; Zabarnick, S.; West, Z. J.; Ervin, J. S.; Edwards, T. Use of Measured Species Class Concentrations With Chemical Kinetic Modelling for the Prediction of Autoxidation and Deposition of Jet Fuels. *Energy & Fuels* **2007**, *21*, 530–544.

(8) Bessee, G. B.; Wilson, G. R.; O'Brien, S. *Storage Stability of Jet Fuel not Containing Anti Oxidant(AO), Interim Report, TFLRF No.42,*; 2012.

(9) Pickard, J. M.; Jones, E. G. Catalysis of Jet-A Fuel Autoxidation by Fe_2O_3. *Energy & Fuels* **1997**, *11*, 1232–1236.

(10) Zabarnick, S.; Mick, M. S. Inhibition of Jet Fuel Oxidation by Addition of Hydroperoxide-Decomposing Species. *Industrial & Engineering Chemistry Research* **1999**, 3557–3563.

(11) Alborzi, E.; Gadsby, P.; Ismail, M. S.; Sheikhansari, A.; Dwyer, M. R.; Meijer, A. J. H. M.; Blakey, S. G.; Pourkashanian, M. Comparative Study of the Effect of Fuel Deoxygenation and Polar Species Removal on Jet Fuel Surface Deposition. *Energy & Fuels* **2019**, *33*, 1825–1836.

(12) Bateman, L.; Hughes, H.; Morris, A. Hydroperoxide decomposition in relation to the initiation of radical chain reactions. *Discuss. Faraday Soc.* **1953**, *14*, 190–199.

(13) Azar, M. T.; Leili, M.; Taherkhani, F.; Bhatnagar, A. A comparative study for the removal of aniline from aqueous solutions using modified bentonite and activated carbon. *Desalination and Water Treatment* **2016**, *57*, 24430–24443.

(14) Hegazy, A. K.; Abdel-Ghani, N. T.; El-Chaghaby, G. A. Adsorption of phenol onto activated carbon from Rhazya stricta: determination of the optimal experimental parameters using factorial design. *Applied Water Science* **2014**, *4*, 273–281.

(15) Downarowicz, D. Adsorption characteristics of propan-2-ol vapours on activated carbon Sorbonorit 4 in electrothermal temperature swing adsorption process. *Adsorption* **2015**, *21*, 87–98.

(16) Qi, N.; LeVan, M. D. Coadsorption of Organic Compounds and Water Vapor on BPL Activated Carbon. 5. Methyl Ethyl Ketone, Methyl Isobutyl Ketone, Toluene, and Modeling. *Industrial & Engineering Chemistry Research* **2005**, *44*, 3733–3741.

(17) da Silva, A. H.; Miranda, E. A. Adsorption/Desorption of Organic Acids onto Different Adsorbents for Their Recovery from Fermentation Broths. *Journal of Chemical & Engineering Data* **2013**, *58*, 1454–1463.

(18) Alslaibi, T. M.; Abustan, I.; Ahmad, M. A.; Foul, A. A. Kinetics and equilibrium adsorption of iron (II), lead (II), and copper (II) onto activated carbon prepared from olive stone waste. *Desalination and Water Treatment* **2014**, *52*, 7887–7897.

(19) Prasad, G. K.; Singh, B.; Saradhi, U. V. R.; Suryanarayana, M. V. S.; Pandey, D. Adsorption and Reaction of Diethyl Sulfide on Active Carbons with and without Impregnants under Static Conditions. *Langmuir* **2002**, *18*, 4300–4306.

(20) Striebich, R. C.; Contreras, J.; Balster, L. M.; West, Z.; Shafer, L. M.; Zabarnick, S. Identification of Polar Species in Aviation Fuels using Multidimensional Gas Chromatography-Time of Flight Mass Spectrometry. *Energy & Fuels* **2009**, *23*, 5474–5482.

(21) West, Z. J.; Zabarnick, S.; Striebich, R. C. Determination of Hydroperoxides in Jet Fuel via Reaction with Triphenylphosphine. *Industrial & Engineering Chemistry Research* **2005**, *44*, 3377–3383.

(22) *Handbook of Aviation Fuel Properties*, 4th ed.; Coordinating Research Council, 2014.

(23) Frisch, M. J. et al. Gaussian 16 Revision C.01. 2016; Gaussian Inc. Wallingford CT.

(24) Dunning, T. H. Gaussian basis sets for use in correlated molecular calculations. I. The atoms boron through neon and hydrogen. *The Journal of Chemical Physics* **1989**, *90*, 1007–1023.

(25) Kendall, R. A.; Dunning, T. H.; Harrison, R. J. Electron affinities of the first-row atoms revisited. Systematic basis sets and wave functions. *The Journal of Chemical Physics* **1992**, *96*, 6796–6806.

(26) Becke, A. D. Density-functional thermochemistry. III. The role of exact exchange. *The Journal of Chemical Physics* **1993**, *98*, 5648–5652.

(27) Woon, D. E.; Dunning, T. H. Gaussian basis sets for use in correlated molecular calculations. III. The atoms aluminum through argon. *The Journal of Chemical Physics* **1993**, *98*, 1358–1371.

(28) Peterson, K. A.; Woon, D. E.; Dunning, T. H. Benchmark calculations with correlated molecular wave functions. IV. The classical barrier height of the H+H2=H2+H reaction. *The Journal of Chemical Physics* **1994**, *100*, 7410–7415.

(29) Wilson, A. K.; van Mourik, T.; Dunning, T. H. Gaussian basis sets for use in correlated molecular calculations. VI. Sextuple zeta correlation consistent basis sets for boron through neon. *Journal of Molecular Structure: THEOCHEM* **1996**, *388*, 339–349.

(30) Tomasi, J.; Mennucci, B.; Cammi, R. Quantum mechanical continuum solvation models. *Chemical Reviews* **2005**, *105*, 2999–3093.

(31) Dolg, M. Chapter 14 - Relativistic Effective Core Potentials. *Theoretical and Computational Chemistry* **2002**, *11*, 793–862.

(32) Cossi, M.; Barone, V. Analytical second derivatives of the free energy in solution by polarizable continuum models. *J. Chem. Phys.* **1998**, *109*, 6246–6254.

(33) Cances, E.; Mennucci, B.; Tomasi, J. A new integral equation formalism for the polarizable continuum model: Theoretical background and applications to isotropic and anisotropic dielectrics. *J. Chem. Phys.* **1997**, *107*, 3032–3041.

(34) Grimme, S. Supramolecular binding thermodynamics by dispersion-corrected density functional theory. *Chemistry–A European Journal* **2012**, *18*, 9955–9964.

(35) Funes-Ardoiz, I.; Paton, R. GoodVibes. *version 2:03* **2009**, *Zenodo*.

(36) Bach, R.; Dmitrenko, O. Electronic Requirements for Oxygen Atom Transfer from Alkyl Hydroperoxides. Model Studies on Multisubstrate Flavin-Containing Monooxygenases. *J. Phys. Chem. B* **2003**, *107*, 12851–12861.

(37) Zabarnick, S.; Phelps, D. Density Functional Theory Calculations of the Energetics and Kinetics of Jet Fuel Autoxidation Reaction. *Energy & Fuels* **2006**, *20*, 488–497.

(38) Zou., L.; Shen, K.; Fu, Y.; Guo, Q. Initiation of petroleum formation and antioxidant function, a DFT study of sulfur-sulfur bond dissociation enthalpies. **2007**, *20*, 754–763.

(39) Roux, M.; Foces-Foces, C.; Notario, R.; da Silva, M. A. V. R.; da Silva, M. d. D. M. C. R.; Santos, A. F. L. O. M.; Juaristi, E. Experimental and Computational Thermochemical Study of Sulfur Containing Amino Acids: l-Cysteine, l-Cystine, and l-Cysteine Derived Radicals. S-S, S-H, and C-S Bond Dissociation Enthalpies. *J. Phys. Chem.* **2010**, *114*, 10530–10540.

(40) Yang., Y. M.; Yu., H. Z.; Sun., X. H.; Dang, Z. M. Density Functional Theory Calculations on S-S Bond Dissociation Energies of Disulfides. *J. Phys. Org. Chem.* **2016**, *29*, 6–13.